Experimental and numerical characterization of a lean premixed flame stabilized by nanosecond discharges

Victorien Blanchard, Nicolas Minesi, Yacine Bechane, Benoit Fiorina, Christophe O Laux

AIAA SciTech Forum
January 3-7, 2022, San Diego, CA & Virtual
AIAA SCITECH 2022 Forum

10.2514/6.2022-2255

Experimental and Numerical Characterization of a Lean Turbulent Premixed Flame Stabilized by Nanosecond Discharges

Victorien P. Blanchard[1], Nicolas Q. Minesi[2], Yacine Bechane[3], Benoît Fiorina[4] and Christophe O. Laux[5]
Laboratoire EM2C, CNRS, CentraleSupélec, Université Paris-Saclay, 3, rue Joliot-Curie, 91190 Gif-sur-Yvette Cedex

This article presents a joint experimental and numerical analysis of a lean turbulent premixed methane-air flame stabilized by nanosecond repetitively pulsed discharges. In the experiments, the transient effects of the discharge on combustion are quantified by optical diagnostics to characterize their impact on flame stabilization. The flame shape is studied with OH* chemiluminescence imaging and the temperature is measured by optical emission spectroscopy. In parallel, Large Eddy Simulation (LES) of the turbulent premixed flame is conducted. Combustion chemistry is modeled by an analytically reduced mechanism whereas the plasma discharge is described by a semi-empirical model. The comparison between experiments and simulations validates the numerical methodology.

I. Introduction

Over 80% of primary energy production worldwide relies on the combustion of hydrocarbon fuels and cannot be replaced in the short term by carbon free sources in many industrial processes. Combustion is also responsible for pollutant emissions such as carbon monoxide, nitric oxides, sulfur oxides, soot, and particulate matter. A strategy to mitigate pollutant formation consist in burning lean premixed fuel-air mixtures. In that case, the flame temperature is lower than under stoichiometric conditions, which limits the formation of pollutants such as soot, carbon monoxide and NO_x. Lean combustion, however, is subject to instabilities and blowout and needs to be stabilized for reliable combustion.

A promising way is to apply electrical discharges [1–3], and especially nanosecond repetitively pulsed discharges [4–5]. This type of discharges is generally out of equilibrium and can efficiently produce radicals, which promote combustion at a low power budget [6–8]. It was shown in previous works that nanosecond discharges can extend the lean blowout limits of a bluff-body burner [9] as well as swirl-stabilized burners [10–13]. The ability of nanosecond discharges to stabilize lean flames was confirmed experimentally for both gaseous and liquid fuels [11], for thermal power up to 50 kW [12], and also at high-pressure up to 5 bar [13–14].

[1] Ph.D. Student, AIAA Member
[2] Postdoctoral researcher, AIAA Member
[3] Ph.D. Student
[4] Professor
[5] Professor, AIAA Fellow

To explain the plasma effects on combustion, experimental studies seek to measure temperature and species densities in air or fuel-air mixtures. Experimental kinetic studies are carried out to validate kinetic mechanisms and to identify the main pathways of radicals formation and their interaction with the fuel and oxidizer molecules [6,15–24]. Plasma-assisted combustion simulations, with detailed chemistry are mainly limited to 0D or 1D configurations, because of computational cost constraints.

2D numerical simulations have been performed for H_2-air ignition by a nanosecond discharge [25–26] with detailed plasma and combustion chemistry, resolution of the Poisson equation, and of the flow motion. These studies are of importance to investigate the interaction of the discharge species with the gas as well as local and non-uniform spatial effects. However, their implementation remains computationally too expensive for simulating repetitive discharges. To circumvent this problem, Bak and Cappelli [27] proposed 2D simulations where the electric field is not resolved but considered homogenous between the electrodes. They were able to simulate a laminar methane-air flame stabilized by nanosecond discharges applied at 30 kHz. It is however still very challenging to employ detailed plasma chemistry for 3D simulations of turbulent combustion.

One of the species generally produced by plasma discharges in fuel-air mixtures is ozone. To isolate its effect on a turbulent flame, Ehn *et al.* [28] studied a flame with O_3-enrichment and compared the experimental results with 3D high-fidelity turbulent combustion simulations. However, this method has not permitted to perform simulations with a detailed description of all the physical and chemical phenomena occurring in plasma-assisted combustion.

Therefore, direct coupling of Computational Fluid Dynamics (CFD) with detailed plasma-combustion kinetic is too expensive to study 3-D phenomena involved when a turbulent flame interacts with a large number of repetitive discharges [29–31].

For that reason, Castela *et al.* [32] developed a reduced analytical model for nanosecond discharge. This model predicts the fraction of discharge energy spent on fast gas heating, vibrational heating, and fast dissociation of molecular oxygen [8,21]. Initially applied to study plasma-induced ignition of quiescent flow [33], it was recently implemented in a Large Eddy Simulation (LES) solver [34] to study ignition of a premixed turbulent methane-air flames by a series of nanosecond repetitively pulsed discharges [35]. The development of such models is necessary to perform plasma-assisted combustion simulations in industrial applications where accurate and reliable numerical tools are needed to design innovative combustion chambers and plasma reactors.

The goal of this study is to present an experimental case of lean flame stabilization to assess the ability of numerical models to reproduced plasma-assisted flames in laboratory and industrial burners. Preliminary numerical results will be compared to experiments in order to validate the model of nanosecond discharge [32,35].

II. Experimental setup and numerical modeling

A. Experimental setup and diagnostics

Experiments are carried out with a bluff-body burner represented in Fig. 1. Methane and air are premixed in a chamber before being supplied at the bottom of the burner. A cylindrical bluff-body is placed concentrically within the annular injection duct and acts as a flame holder. The outer diameter of the bluff-body and the inner diameter of the injection duct are 10 mm and 16 mm, respectively. A recirculation zone is created downstream of the bluff-body. In this zone, the residence time is long enough for the combustion to occur. The air flow rate is set to 16 Nm^3/h and the methane flow rate to 1.34 Nm^3/h. The equivalence ratio is thus 0.8 for a theoretical flame thermal power of 13.3 kW. The bulk velocity corresponding to this gas flow rate is $v_{bulk} = 43.3\ m.s^{-1}$ which give a Reynolds number based on the hydraulic diameter $Re = 1.6\ 10^4$. The flow is in a fully developed turbulent regime at the outlet of the injection duct.

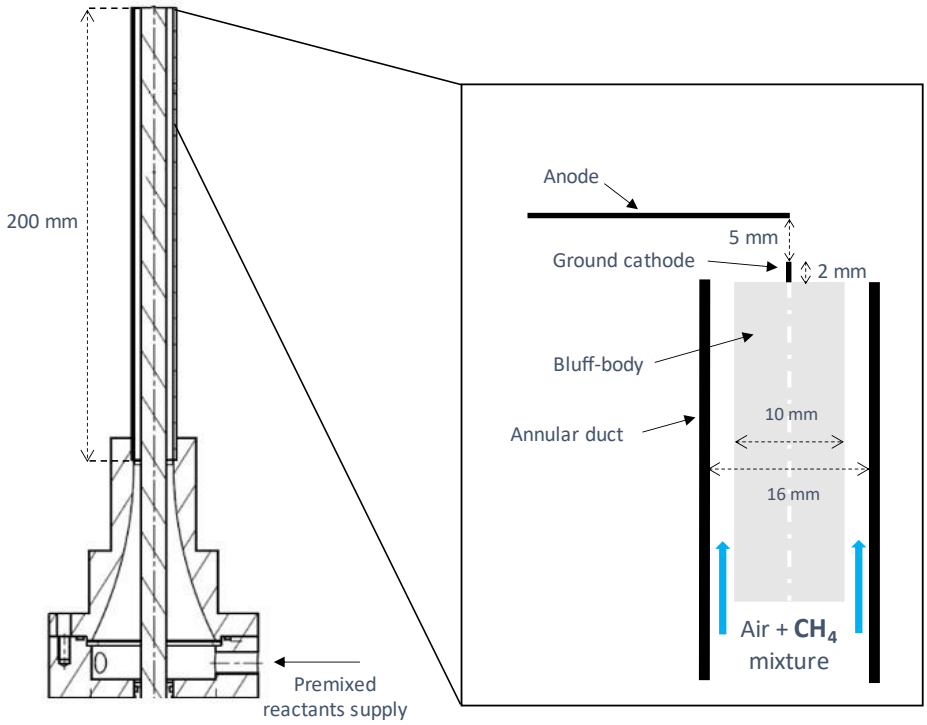

Fig. 1 Schematic of the bluff-body burner with electrodes.

The 2-mm vertical ground cathode is centered on top of the bluff-body and the horizontal anode is located 5-mm above. Nanosecond discharges are generated across the 5-mm gap by 10-ns duration high-voltage pulses delivered by a pulse generator (FID Technology model FPG 10-30NM10). Voltage and current are measured with electrical probes (Lecroy PPE 20kV, Pearson current monitor model 6585) connected to an oscilloscope (TeledyneLecroy HDO 6104) to monitor the energy deposited by each discharge pulse.

In this work, the steady-state deposited energy is fixed at 1.8 mJ per pulse and the discharges are applied at a repetition frequency of 20 kHz. The ratio of electric power over flame thermal power is therefore 0.3 %. The non-assisted flame and the flame with plasma are shown in Fig. 2.

Fig. 2 Photographs of the lean flame (Φ = 0.8) without (left) and with (right) 1.8-mJ nanosecond discharges applied at 20 kHz.

OH* chemiluminescence images of the flame are recorded using an ICCD camera (Princeton Instruments, inc. I-MAX-512-T, 18/G/II) fitted with a UV-Nikkor 105 mm lens (f /4.5) and an interference bandpass filter (Asahi Spectra Optical Filters ZHQA310) centered at 310 nm (FWHM = 10 nm) to collect the spontaneous emission of the OH(A-X) transition. Images are acquired with a 48-µs time gate between consecutive discharges to avoid direct discharge emission. All the OH* chemiluminescent intensity images presented in this work are averaged over 1000 samples.

The N_2(C) rotational temperature is measured by Optical Emission Spectroscopy (OES) using a monochromator (ActonSpectra 2500i) coupled to an ICCD camera (Roper Scientific I-MAX-512-T, 18/G/II). The discharge emission is collected through the entrance slit with two spherical lenses of 100-mm focal distance. A longpass interference filter with a cut-off wavelength at 300 nm (UV Melles Griot 03 FCG 121 WG 305) is inserted into the optical path to avoid second-order emission of species emitting in the UV. Spectra are acquired using a 2400-gr.mm^{-1} grating blazed at 150 nm with a spectral resolution of 0.065 nm. Experimental spectra are collected during a 2-ns time gate with a few hundreds on-CCD accumulations depending on the intensity of the signal. The experimental setup for OES is presented in Fig. 3. Experimental spectra of the N_2(C→B) (0,2) and (1,3) vibrational bands are fitted with the line-by-line radiation solver SPECAIR [36] to determine the rotational temperature during the burst of discharges as done in [37].

B. Numerical modeling

Large Eddy Simulation (LES) are performed with YALES2, an unstructured finite-volume low-Mach number code dedicated to high-performance computing of reactive flows [34]. Details of the combustion kinetic mechanism, turbulence model, numerical schemes, space domain and mesh are given in [35]. The discharge is assumed to be a cylinder with a length of 5 mm and a radius of 0.6 mm. In this model [32,35], the canonical set of equations solved by the combustion solver is modified to reproduce the main discharge effects. The main principles are summarized here. It is assumed that the discharge energy is partitioned into three channels: ultra-fast heating, ultra-fast dissociation of oxygen molecules and ultra-fast vibrational excitation of nitrogen molecules responsible for slow heating due to VT relaxation. In addition to the filtered Navier Stokes and species equations, the YALES2 code solves a conservation equation of vibrational energy. Source terms are added to the mass-species balance equations to account for the dissociation of oxygen molecules and production of atomic oxygen during the discharge. Source terms are also added

to the energy conservation equation to account for the variation of chemical energy and ultra-fast heating. The total energy equation and the vibrational energy equation are coupled by a relaxation term for the vibrational energy. Details of the plasma-combustion model along with its implementation in YALES2 are given in [32,35].

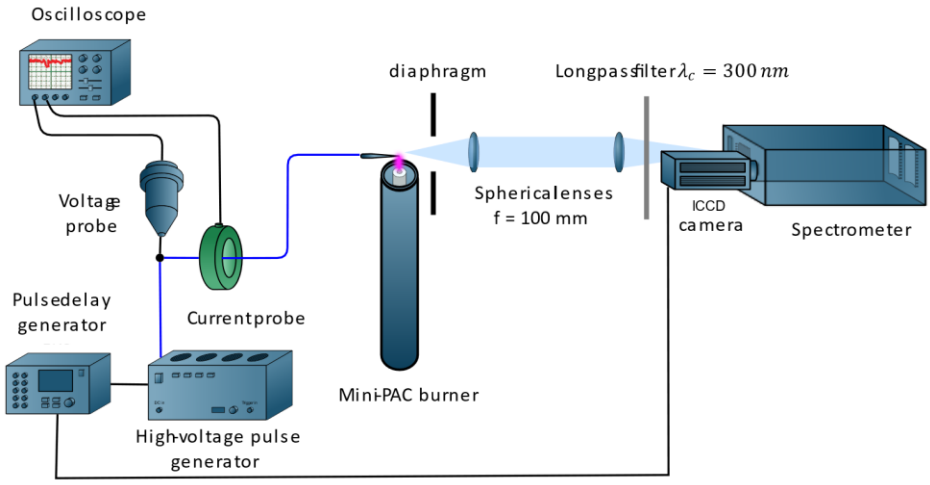

Fig. 3 Bluff-body burner, electrical, and OES experimental setup.

C. Model validation strategy

To validate models, a wide range of experimental conditions is required. A single experiment is most of the time not sufficient to fulfil this task. For instance, ignition experiments are not sufficient to validate the effects of repetitive discharges. Moreover, the goal of plasma-assisted ignition is to efficiently initiate the combustion chain-branching reactions. In practical applications, ignition is performed in stoichiometric or rich conditions.

On the other hand, plasma-assisted stabilization of lean flames is expected to sustain these chain-branching reactions in conditions where they normally terminate without plasma. This is achieved by applying discharges at a repetition frequency of a few tens of kHz. These experiments can provide model testing in steady state (forced regime) conditions. But they are not suitable to test the ability of the model to reproduce the effect of a single discharge or of a reduced number of discharges.

In this work we propose an experiment to assess not only the ability of a model to reproduce the effects of a reduced number of discharges, as in ignition experiments, but also to reproduce steady state conditions when discharges are applied continuously.

The chosen operating conditions of the burner for the experiment presented in this paper are in the vicinity of the lean flammability limit, as shown in Fig. 2. The flame is confined to the recirculation zone downstream of the bluff-body and a large fraction of the gas is not burnt. To understand and quantify the plasma effect on the combustion, a burst of 5000 discharges is applied in this weak flame. A strong effect is observed, as shown in Fig. 2. The transient regime from the weak flame to the stabilized flame and the steady state regime are experimentally characterized and compared with numerical simulations. The accuracy of the model is therefore tested on both short timescales, with the transient effects of the first discharges, and on longer timescale, i.e. steady state conditions at the end of the burst.

III. Results and discussion

A. Electrical characterization of the burst of discharges

The averaged current and voltage traces of the high-voltage pulse are represented in Fig. 4 along with the calculated energy when discharges are applied continuously at 20 kHz. Due to the impedance mismatch between the cable, the plasma, and the pulse generator, several reflections occur at the electrode and also at the pulser output. About 75% of the total energy is deposited by the incident pulse and the remaining energy is deposited within 300 ns by the reflections. The total energy dissipated into the plasma is 1.8 mJ. The probes are located halfway on the coaxial cable, the energy that is not deposited is reflected which explains the succession of energy increase and decrease with each reflection.

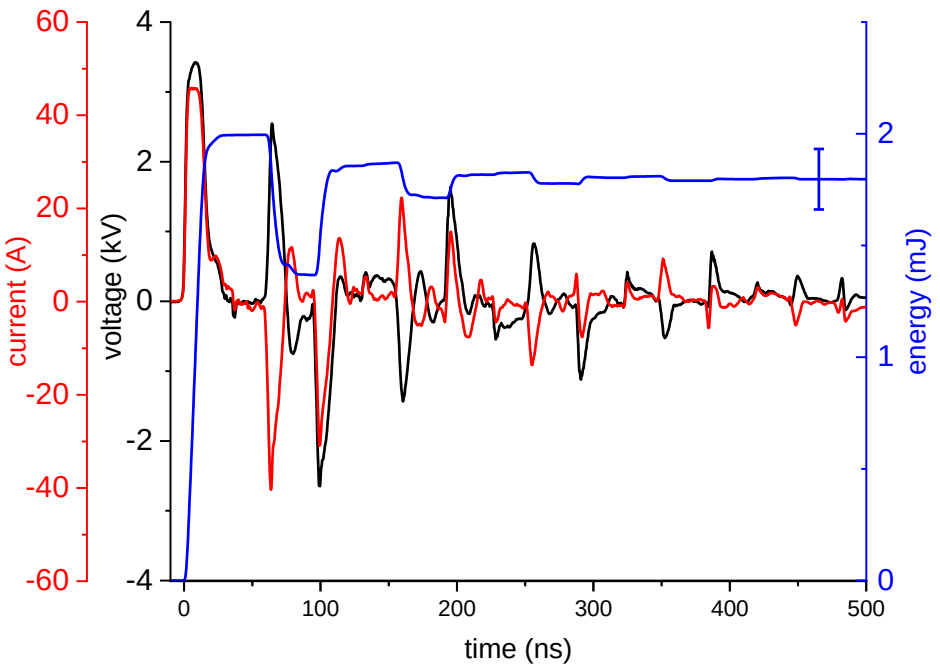

Fig. 4 Current (red) and voltage (black) traces measured along the coaxial cable and deposited energy (blue). The traces are averaged over 10 000 samples.

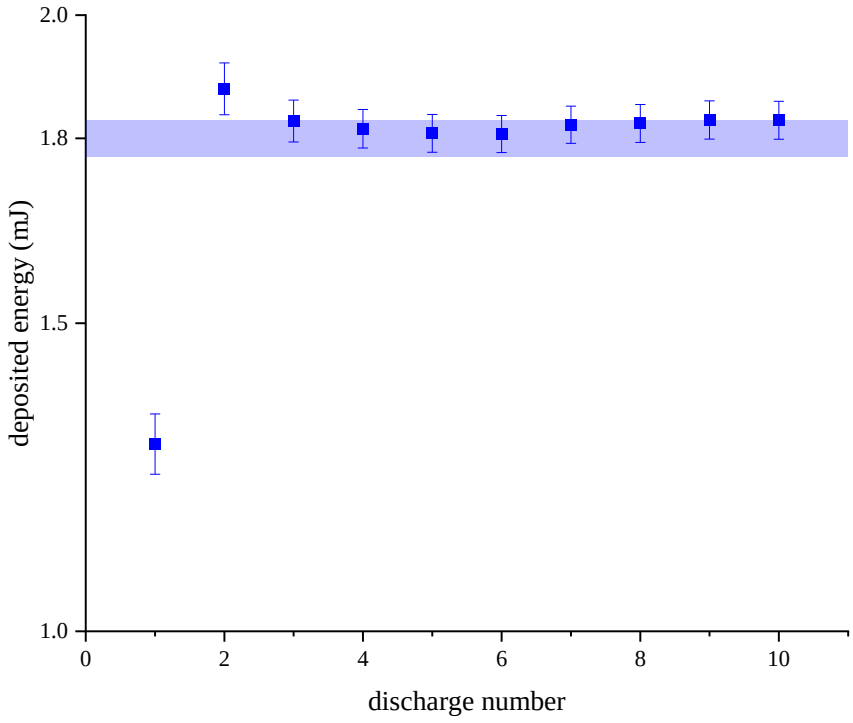

Fig. 5 Evolution of total deposited energy for the first 10 discharges of the burst. The blue strip corresponds to an energy of 1.8 ± 0.03 mJ.

Fig. 5 shows the total energy deposited by these discharges. The high-voltage pulse generator used in this study is very stable in continuous mode but, as shown in Fig. 5, the first discharge exhibits a voltage undershoot and the second discharge a slight voltage overshoot. Therefore, in the numerical simulation, we set the deposited energy of the first two discharges to 1.30 and 1.88 mJ. The steady-state deposited energy was set to 1.80 mJ.

B. Flame shape development during the burst of discharges

As presented in Fig. 2, the weak flame without plasma is confined to the recirculation zone downstream of the bluff-body. However, when NRP discharges are applied, the flame stabilizes even though the bulk velocity of the flow is high.

In Refs. [37–38], the discharge emission was characterized at steady state (i.e. with discharges continuously applied at 20 kHz). In this work, we study the stabilization mechanism and the transition between the weak flame and the plasma-stabilized flame. This is illustrated in Fig. 6 with direct visualization of OH* chemiluminescence. The first image corresponds to the weak flame without discharge. The following images present the flame shape evolution during the burst of discharges. The flame contour is delimited by the intensity threshold obtained with Otsu's method [39] applied to the Abel-inverted image of the weak flame without plasma. This threshold value is then used for all Abel-inverted images. From this contour, we extract the flame height above burner (HAB) plotted in Fig. 7. During the first millisecond (i.e. until discharge 20) the plasma chemistry has no effect on the flame shape. Then the flame develops during 4 ms and reaches a steady state after approximately 100 discharges. It was estimated in a previous study that the residence time in the recirculation zone for an air flow rate of 15 Nm^3/h is about 0.8 ms [40]. This matches well the characteristic time of 1 ms at the beginning of the burst of discharges (i.e. until discharge 20). We can thus infer that the heat and radicals produced by the discharges contribute directly to the flame front propagation as soon as they reach the shear layer of the recirculation zone. The fresh gases that were not burnt without plasma are ignited and the flame front propagates farther downstream of the bluff-body.

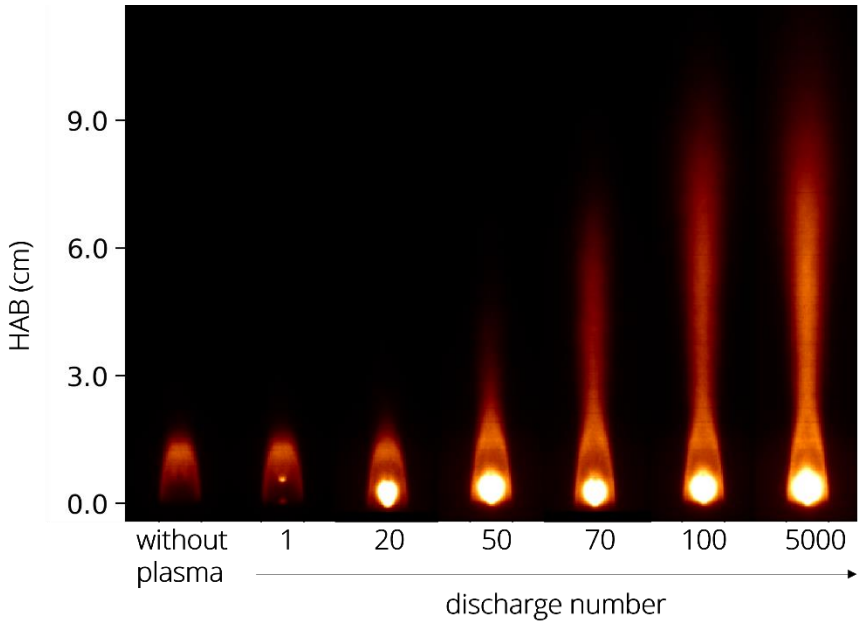

Fig. 6 Direct visualization of OH* chemiluminescence images of the flame during the stabilization when a burst of discharges is applied.

This behavior can be interpreted in terms of vorticity generation in the wake of the bluff-body. Without plasma, the vorticity generated by the shear layer of the bluff-body tends to extinguish the flame [41]. In the present study, as we are close to lean blow out, the vorticity constrains the combustion to the recirculation zone downstream of the bluff-body. According to Shanbhogue et al. [41], in the case of a reacting flow, the exothermicity tends to generate vorticity of opposite sign, which enables the flame to open and propagate outside the recirculation zone as shown in Fig. 6.

The flame development exhibits two characteristic times: the first one, 1 ms, corresponds to the time needed for the flame to respond to the application of discharges. We see in Fig. 6 that even though there is no macroscopic effect on the flame, i.e. no change in the flame shape, the OH* chemiluminescent intensity strongly increases in the recirculation zone. This shows that there is a strong chemical and thermal activity in this zone. The second characteristic time scale evidenced by these images is the time necessary for the flame to develop and stabilize. This time is equal to approximately 5 ms. The flame height evolution plotted in Fig. 7 provides four quantities to validate numerical simulations: two characteristic times and two flame heights to assess both the dynamics and the flame shape.

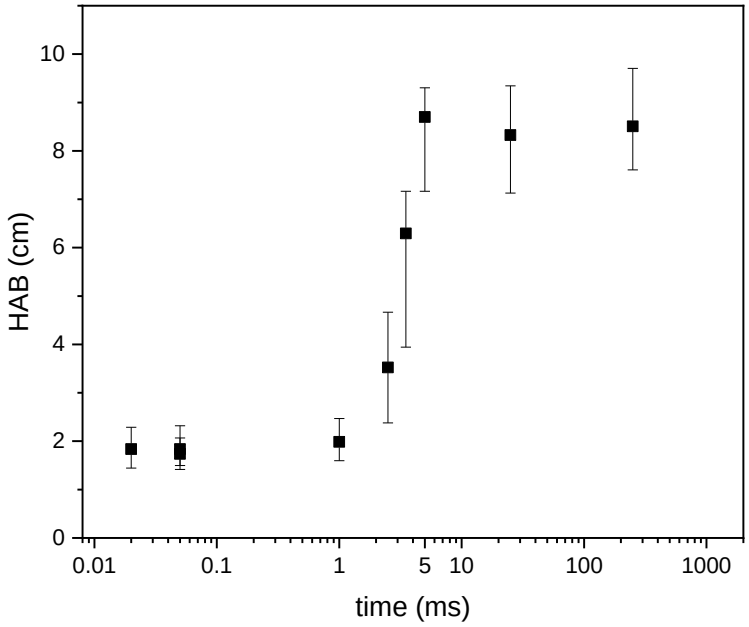

Fig. 7 Flame height above burner during the burst of discharges. The height is determined from Otsu's contours of Abel inverted mean OH* chemiluminescence images.

C. Temperature evolution during the burst of discharges

For each discharge we acquire spectra over a temporal window of 2 ns with a step of 1 ns to track the evolution of the rotational temperature of $N_2(C)$. A typical experimental spectrum fitted with the line-by-line radiation code SPECAIR [36] is shown in Fig. 8. An example of the temperature evolution during the 10^{th} discharge of the burst is plotted in Fig. 9. For this discharge, we observe a temperature increase of approximately 350 K within 15 ns. Time t = 0 ns is defined as the rising half-maximum of the discharge broadband emission during the high-voltage pulse. For times later than 14 ns, the number density of $N_2(C)$ being very low, the signal intensity does not allow to fit the spectra. It was not possible to determine the rotational temperature evolution after that time in this experiment.

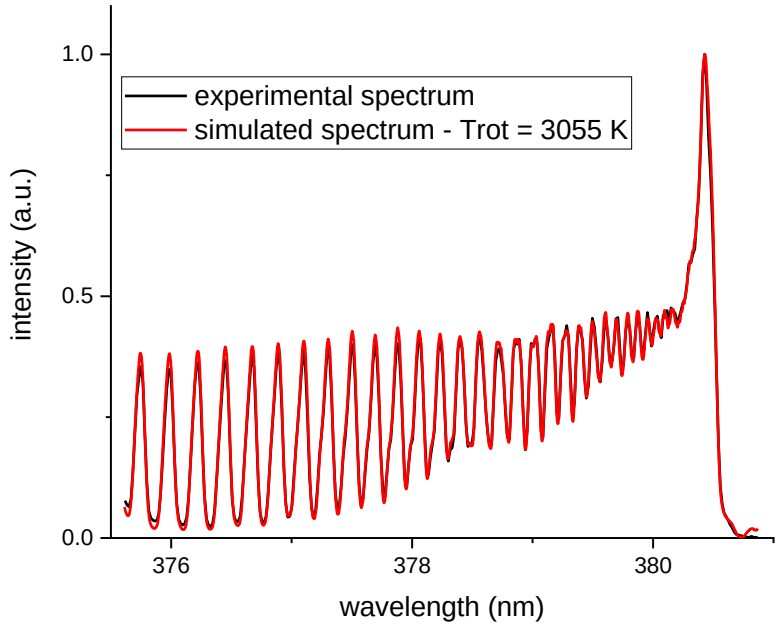

Fig. 8 Determination of the rotational temperature of $N_2(C)$ by fitting the normalized experimental spectrum with SPECAIR

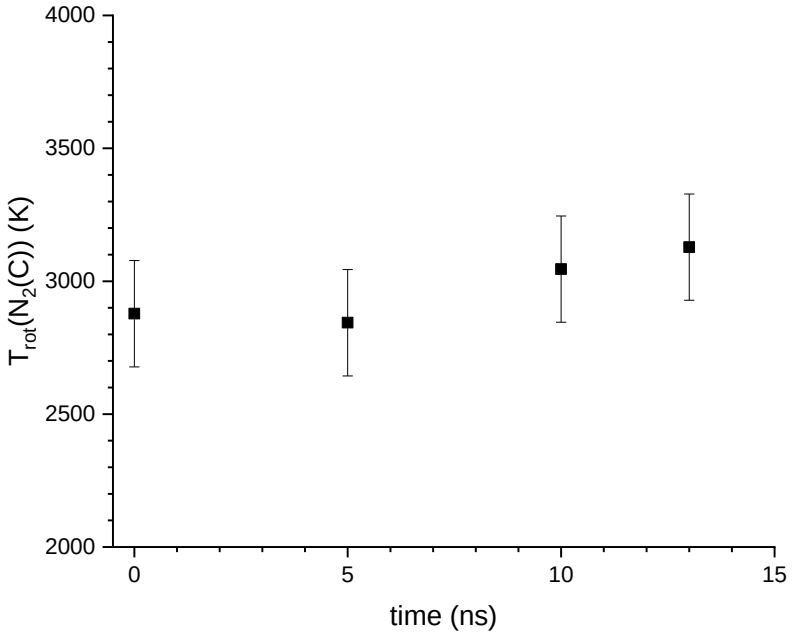

Fig. 9 Evolution of the rotational temperature of $N_2(C)$ during the 10th discharge of the burst. Spectra are measured in the middle of the interelectrode gap.

According to Refs. [8,38], the rotational temperature of $N_2(C)$ at the beginning of the discharge is proportional to the gas translational temperature. $N_2(C)$ is mainly populated from the ground state by electron impact reactions at the beginning of the discharge. The rotational number is conserved through these reactions and thus the rotational temperature of $N_2(C)$ is proportional to the rotational temperature of $N_2(C)$ through the ratio of the rotational constants, denoted θ_{rot}^{X} and θ_{rot}^{C}. Finally, the authors in [8,40] show that the rotational temperature of $N_2(X)$ is equilibrated with the translational temperature, leading to:

$$T_{gas} = T_{rot,N_2(X)} = T_{rot,N_2(C)} \times \frac{\theta_{rot}^{X}}{\theta_{rot}^{C}} = 1.12\, T_{rot,N_2(C)} \qquad \text{Eq. 1}$$

We note that rotational relaxation could bring the measured rotational temperature of $N_2(C)$ closer to the gas temperature. However, the rotational relaxation time scales are a few nanoseconds, and therefore full relaxation may not occur. In any case, the measured rotational temperature of $N_2(C)$ is within about 10% of the rotational temperature [8,40].

To compare these measurements with the numerical results, we select for each discharge the temperature at time t = 0 ns because at this time the discharge has not heated the gas and Eq. 1 is verified. During the burst of discharges, we can then plot the evolution of the gas temperature, as shown in Fig. 9.

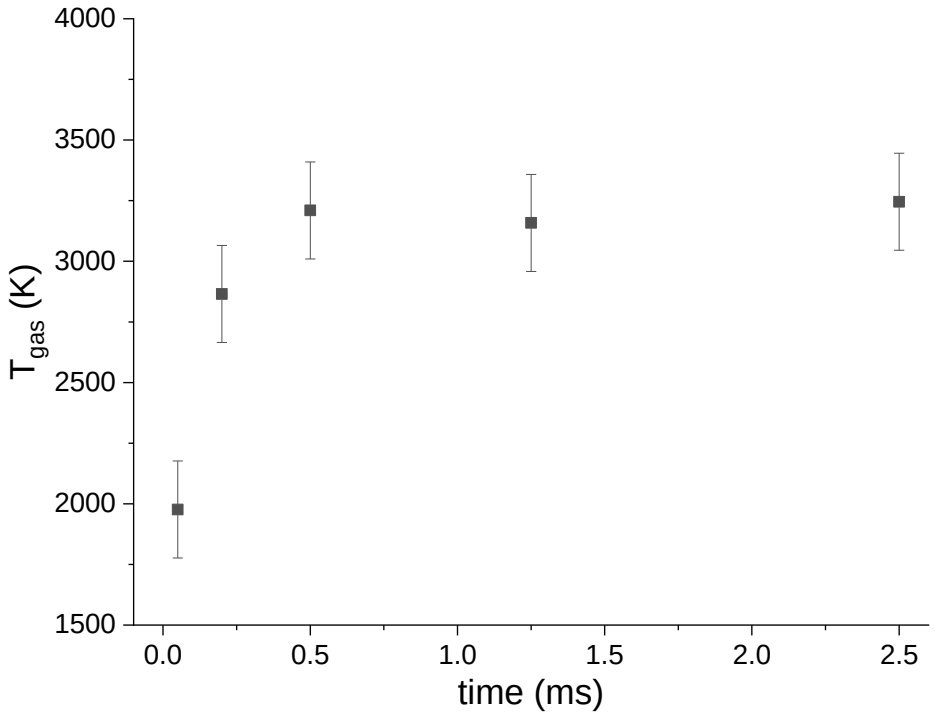

Fig. 10 Evolution of the gas temperature deduced from the rotational temperature of $N_2(C)$ at the beginning of each discharge.

The temperature measured at the beginning of discharge 1 corresponds to the flame temperature without plasma. In our conditions, the adiabatic flame temperature is 1992 K which is consistent with the temperatures measured at the beginning of discharges 1.

The cumulative effects of the discharges are shown in Fig. 10. The train of discharges at 20 kHz is responsible for a temperature increase of 1250 K in approximately 0.5 ms (i.e.10 discharges). This is another interesting characteristic time to validate numerical results. After discharge 10, a steady gas temperature is reached.

IV.Validation of numerical simulations against experiments

In this section, we present preliminary simulations of the experiment and then compare the simulation results with the experimental ones. These simulations were obtained with a model of turbulent plasma-assisted combustion developed by Bechane [35,42]. In Fig. 11, we compare the direct visualization of the OH* chemiluminescence with the simulated OH mass fraction. In the first case on the left, the flame shape without plasma is well captured by the LES solver [34]. The figure on the right shows numerical simulations with the discharges continuously applied (steady state regime). For these simulations, the numerical image is time-averaged from discharge 700 to discharge 900. Comparison of the experimental and simulated images show that the model predicts the shape and length of the plasma-assisted flame remarkably well.

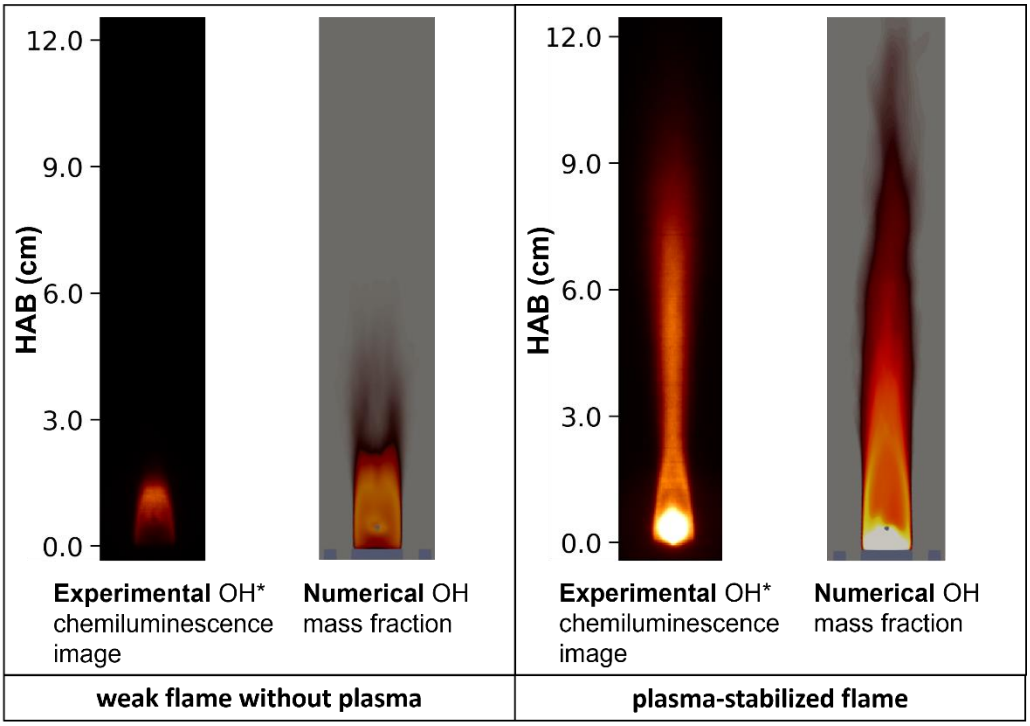

Fig. 11 Comparison of experimental direct visualization of OH* chemiluminescence images with numerical OH mass fraction without plasma (left) and with discharges continuously applied at 20 kHz (right).

The results in Fig. 11 (right) are obtained when steady pulsing is applied. To further validate the model, we now consider the transient regime, i.e. the stabilization process during the burst of discharges to assess the ability of the model to capture the dynamics of the plasma interaction with the flame. The black squares in Fig. 12 correspond to the temperature measurements of Fig. 10 and the red circle corresponds to the temperature predicted by the simulation at the same location and at the same time. As shown in Fig. 12, the pulse to pulse evolution of the gas temperature is very well captured by the simulation. The temperature increase over the first 10 discharges is indeed well predicted and the steady state value is also close to the measured one. The two-step model of fast gas heating and O_2 dissociation [32,35] thus appears reliable to perform numerical simulations of plasma-assisted combustion.

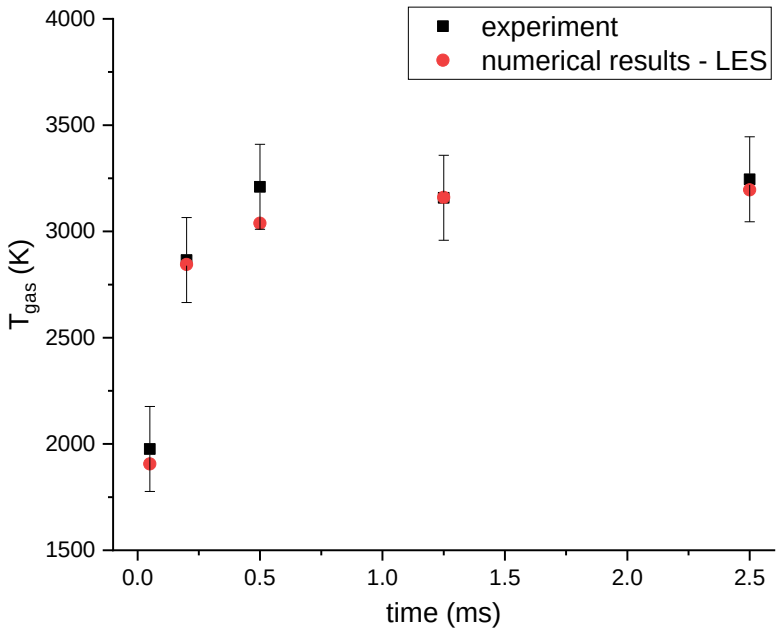

Fig. 12 Comparison of the experimental (black symbols) and numerical temperature (red symbols) evolution in the discharge region during the stabilization sequence.

V. Conclusions

A burst of 5000 NRP discharges is applied at 20 kHz in a lean premixed methane-air flame close to extinction. The stabilization process is first studied by OH* chemiluminescence to characterize the flame shape evolution. It is found that the stabilization time scale depends on the residence time in the recirculation zone downstream of the bluff-body. Then the temperature evolution in the discharge region is measured during the burst of discharges and shows a characteristic time scale of the same order of magnitude. A reduced-order plasma model previously implemented in a LES solver and used to simulate the experiment provides very good results and is able to reproduce the flame dynamics and temperature evolution under the effect of repetitive nanosecond discharges.

Acknowledgments

This work was funded by the ANR grant PASTEC ANR16-CE22-0005. N Minesi has been supported by an IDEX PhD fellowship, ANR-11-IDEX-0003. The authors would like to thank Cécile Oriot for the photographs of Fig. 2, and Erika Jean-Bart and, Yannick Le Teno for technical assistance with the Mini-PAC burner.

References

1. A. Starikovskiy & N. Aleksandrov, Plasma-assisted ignition and combustion. *Progress in Energy and Combustion Science*, **39** (2013) 61–110. https://doi.org/10.1016/j.pecs.2012.05.003.
2. S. M. Starikovskaia, Plasma-assisted ignition and combustion: Nanosecond discharges and development of kinetic mechanisms. *Journal of Physics D: Applied Physics*, **47** (2014). https://doi.org/10.1088/0022-3727/47/35/353001.
3. Y. Ju & W. Sun, Plasma assisted combustion: Dynamics and chemistry. *Progress in Energy and Combustion Science*, **48** (2015) 21–83. https://doi.org/10.1016/j.pecs.2014.12.002.
4. C. H. Kruger, C. O. Laux, L. Yu, D. M. Packan, & L. Pierrot, Nonequilibrium discharges in air and nitrogen plasmas at atmospheric pressure. *Pure and Applied Chemistry*, **74** (2002) 337–347. https://doi.org/10.1351/pac200274030337.
5. D. Z. Pai, D. A. Lacoste, & C. O. Laux, Nanosecond repetitively pulsed discharges in air at atmospheric

pressure—the spark regime. *Plasma Sources Science and Technology*, **19** (2010) 065015. https://doi.org/10.1088/0963-0252/19/6/065015.
6. M. Uddi, N. Jiang, E. Mintusov, I. V Adamovich, & W. R. Lempert, Atomic oxygen measurements in air and air / fuel nanosecond pulse discharges by two photon laser induced fluorescence. *Proceedings of the Combustion Institute*, **32** (2009) 929–936. https://doi.org/10.1016/j.proci.2008.06.049.
7. T. Ombrello, S. H. Won, Y. Ju, & S. Williams, Flame propagation enhancement by plasma excitation of oxygen. Part II: Effects of O2(a1Dg). *Combustion and Flame*, **157** (2010) 1916–1928. https://doi.org/10.1016/j.combustflame.2010.02.004.
8. D. L. Rusterholtz, D. A. Lacoste, G. D. Stancu, D. Z. Pai, & C. O. Laux, Ultrafast heating and oxygen dissociation in atmospheric pressure air by nanosecond repetitively pulsed discharges. *Journal of Physics D: Applied Physics*, **46** (2013). https://doi.org/https://doi.org/10.1088/0022-3727/46/46/464010.
9. G. Pilla, D. Galley, D. A. Lacoste, F. Lacas, D. Veynante, & C. O. Laux, Stabilization of a Turbulent Premixed Flame Using a Nanosecond Repetitively Pulsed Plasma. *IEEE Transactions on Plasma Science*, **34** (2006) 2471–2477. https://doi.org/10.1109/TPS.2006.886081.
10. J. Choe & W. Sun, Blowoff hysteresis, flame morphology and the effect of plasma in a swirling flow. *Journal of Physics D: Applied Physics*, **51** (2018). https://doi.org/10.1088/1361-6463/aad4dc.
11. G. Vignat, N. Minesi, P. R. Soundararajan, D. Durox, A. Renaud, V. Blanchard, C. O. Laux, & S. Candel, Improvement of lean blow out performance of spray and premixed swirled flames using nanosecond repetitively pulsed discharges. *Proceedings of the Combustion Institute*, **38** (2021) 6559–6566. https://doi.org/10.1016/j.proci.2020.06.136.
12. S. Barbosa, G. Pilla, D. A. Lacoste, P. Scouflaire, S. Ducruix, C. O. Laux, & D. Veynante, Influence of nanosecond repetitively pulsed discharges on the stability of a swirled propane/air burner representative of an aeronautical combustor. *Philosophical Transactions of the Royal Society A: Mathematical, Physical and Engineering Sciences*, **373** (2015) 20140335. https://doi.org/10.1098/rsta.2014.0335.
13. F. Di Sabatino & D. A. Lacoste, Enhancement of the lean stability and blow-off limits of methane-air swirl flames at elevated pressures by nanosecond repetitively pulsed discharges. *Journal of Physics D: Applied Physics*, (2020).
14. G. Heid, G. Pilla, R. Lecourt, & D. A. Lacoste, Assisted combustion of an air-kerosene mixture by nanosecond repetitively pulsed discharges. *Isabe* (2009), p. 474.
15. M. Uddi, N. Jiang, I. V. Adamovich, & W. R. Lempert, Nitric oxide density measurements in air and air / fuel nanosecond pulse discharges by laser-induced fluorescence. *Journal of Physics D: Applied Physics*, **42** (2009). https://doi.org/10.1088/0022-3727/42/7/075205.
16. M. S. Bak & M. A. Cappelli, Numerical studies of nitric oxide formation in discharge-stabilized flames of premixed methane / air. *Philosophical Transactions of the Royal Society A-Mathematical Physical and Engineering Sciences*, **373** (2015).
17. J. K. Lefkowitz, P. Guo, A. Rousso, & Y. Ju, Species and temperature measurements of methane oxidation in a nanosecond repetitively pulsed discharge. *Philosophical Transactions of the Royal Society A: Mathematical, Physical and Engineering Sciences*, **373** (2015). https://doi.org/10.1098/rsta.2014.0333.
18. Z. Yin, A. Montello, C. D. Carter, W. R. Lempert, & I. V. Adamovich, Measurements of temperature and hydroxyl radical generation/decay in lean fuel-air mixtures excited by a repetitively pulsed nanosecond discharge. *Combustion and Flame*, **160** (2013) 1594–1608. https://doi.org/10.1016/j.combustflame.2013.03.015.
19. I. Shkurenkov & I. V. Adamovich, Energy balance in nanosecond pulse discharges in nitrogen and air. *Plasma Sources Science and Technology*, **25** (2016). https://doi.org/10.1088/0963-0252/25/1/015021.
20. I. V. Adamovich, T. Li, & W. R. Lempert, Kinetic mechanism of molecular energy transfer and chemical reactions in low-temperature air-fuel plasmas. *Philosophical Transactions of the Royal Society A: Mathematical, Physical and Engineering Sciences*, **373** (2015). https://doi.org/10.1098/rsta.2014.0336.
21. N. A. Popov, Pulsed nanosecond discharge in air at high specific deposited energy: Fast gas heating and active particle production. *Plasma Sources Science and Technology*, **25** (2016). https://doi.org/10.1088/0963-0252/25/4/044003.
22. I. V. Adamovich, I. Choi, N. Jiang, J. H. Kim, S. Keshav, W. R. Lempert, E. Mintusov, M. Nishihara, M. Samimy, & M. Uddi, Plasma assisted ignition and high-speed flow control: Non-thermal and thermal effects. *Plasma Sources Science and Technology*, **18** (2009). https://doi.org/10.1088/0963-0252/18/3/034018.
23. A. A. Tropina, M. Uddi, & Y. Ju, On the effect of nonequilibrium plasma on the minimum ignition energy: Part 2. *IEEE Transactions on Plasma Science*, **39** (2011) 3283–3287. https://doi.org/10.1109/TPS.2011.2160570.

24. W. Sun, M. Uddi, S. H. Won, T. Ombrello, C. Carter, & Y. Ju, Kinetic effects of non-equilibrium plasma-assisted methane oxidation on diffusion flame extinction limits. *Combustion and Flame*, **159** (2012) 221–229. https://doi.org/10.1016/j.combustflame.2011.07.008.
25. F. Tholin, D. A. Lacoste, & A. Bourdon, Influence of fast-heating processes and O atom production by a nanosecond spark discharge on the ignition of a lean H2-air premixed flame. *Combustion and Flame*, **161** (2014) 1235–1246. https://doi.org/10.1016/j.combustflame.2013.11.007.
26. X. Mao, H. Zhong, & Y. Ju, 2D modeling of plasma-assisted H2-air ignition in a nanosecond discharge with detailed chemistry. *AIAA SciTech 2021 Forum* (2021). https://doi.org/https://doi.org/10.2514/6.2021-1790.
27. M. S. Bak, H. Do, M. G. Mungal, & M. A. Cappelli, Plasma-assisted stabilization of laminar premixed methane/air flames around the lean flammability limit. *Combustion and Flame*, **159** (2012) 3128–3137. https://doi.org/10.1016/j.combustflame.2012.03.023.
28. A. Ehn, J. J. Zhu, P. Petersson, Z. S. Li, M. Aldén, C. Fureby, T. Hurtig, N. Zettervall, A. Larsson, & J. Larfeldt, Plasma assisted combustion: Effects of O3 on large scale turbulent combustion studied with laser diagnostics and Large Eddy Simulations. *Proceedings of the Combustion Institute*, **35** (2015) 3487–3495. https://doi.org/10.1016/j.proci.2014.05.092.
29. D. A. Xu, M. N. Shneider, D. A. Lacoste, & C. O. Laux, Thermal and hydrodynamic effects of nanosecond discharges in atmospheric pressure air. *Journal of Physics D: Applied Physics*, **47** (2014). https://doi.org/10.1088/0022-3727/47/23/235202.
30. C. Dumitrache, A. Gallant, N. Minesi, S. Stepanyan, G. D. Stancu, & C. O. Laux, Hydrodynamic regimes induced by nanosecond pulsed discharges in air: Mechanism of vorticity generation. *Journal of Physics D: Applied Physics*, **52** (2019). https://doi.org/10.1088/1361-6463/ab28f9.
31. S. Stepanyan, N. Minesi, A. Tibere-Inglesse, A. Salmon, G. D. Stancu, & C. O. Laux, Spatial evolution of the plasma kernel produced by nanosecond discharges in air. *Journal of Physics D: Applied Physics*, **52** (2019). https://doi.org/10.1088/1361-6463/ab1ba4.
32. M. Castela, B. Fiorina, A. Coussement, O. Gicquel, N. Darabiha, & C. O. Laux, Modelling the impact of non-equilibrium discharges on reactive mixtures for simulations of plasma-assisted ignition in turbulent flows. *Combustion and Flame*, **166** (2016) 133–147. https://doi.org/10.1016/j.combustflame.2016.01.009.
33. M. Castela, S. Stepanyan, B. Fiorina, A. Coussement, O. Gicquel, N. Darabiha, & C. O. Laux, A 3-D DNS and experimental study of the effect of the recirculating flow pattern inside a reactive kernel produced by nanosecond plasma discharges in a methane-air mixture. *Proceedings of the Combustion Institute*, **36** (2017). https://doi.org/10.1016/j.proci.2016.06.174.
34. V. Moureau, P. Domingo, & L. Vervisch, Une algorithmique optimisée pour le supercalcul appliqué à la mécanique des fluides numérique. *Comptes Rendus - Mecanique*, **339** (2011) 141–148. https://doi.org/10.1016/j.crme.2010.12.001.
35. Y. Bechane & B. Fiorina, Numerical investigations of turbulent premixed flame ignition by a series of Nanosecond Repetitively Pulsed discharges. *Proceedings of the Combustion Institute*, **38** (2021) 6575–6582. https://doi.org/10.1016/j.proci.2020.06.258.
36. C. O. Laux, T. G. Spence, C. H. Kruger, & R. N. Zare, Optical diagnostics of atmospheric pressure air plasmas. *Plasma Sources Science and Technology*, **12** (2003) 125–138. https://doi.org/10.1088/0963-0252/12/2/301.
37. V. P. Blanchard, N. Q. Minesi, S. Stepanyan, G.-D. Stancu, & C. O. Laux, Dynamics of a Lean Flame Stabilized by Nanosecond Discharges. *AIAA SciTech 2021 Forum* (2021), pp. 1–10. https://doi.org/10.2514/6.2021-1700.
38. N. Minesi, Thermal spark formation and plasma-assisted combustion by nanosecond repetitive discharges, CentraleSupélec, Université Paris Saclay, 2020.
39. N. Otsu, A Threshold Selection Method from Gray-Level Histograms. *IEEE Transactions on Systems, Man, adn Cybernetics*, **9** (1979) 62–66. https://doi.org/10.1109/TSMC.1979.4310076.
40. G. Pilla, Etude Expérimentale de la Stabilisation de Flammes Propane-Air de Prémélange par Décharges Nanosecondes Impulsionnelles Répétitives, Ecole Centrale Paris, 2008.
41. S. J. Shanbhogue, S. Husain, & T. Lieuwen, Lean blowoff of bluff body stabilized flames: Scaling and dynamics. *Progress in Energy and Combustion Science*, **35** (2009) 98–120. https://doi.org/10.1016/j.pecs.2008.07.003.
42. Y. Bechane, N. Darabiha, V. Moureau, C. Laux, & B. Fiorina, Large eddy simulations of turbulent flame ignition by nanosecond repetitively pulsed discharges. *AIAA Scitech 2019 Forum*, (2019) 1–11. https://doi.org/10.2514/6.2019-0742.